

1 **Global Frictional Equilibrium via Stochastic, Local Coulomb Frictional Slips**

2
3 **Shihuai Zhang and Xiaodong Ma***

4
5 Department of Earth Sciences, ETH Zürich, Zürich, Switzerland

6
7 *Corresponding author: Xiaodong Ma (xiaodongma.rocks@gmail.com)

8 9 **Key Points:**

- 10 • A simple quasi-static 2D model is introduced, quantifying and extending the classic notion
11 of frictional equilibrium of the brittle crust
 - 12 • We investigate the global scale stress evolution due to stochastic, local scale frictional slips
13 in the crustal rock masses
 - 14 • Frictional equilibrium of a stochastic system is greatly affected by its intrinsic friction
15 heterogeneity
- 16

17 Abstract

18 Natural variability of fault friction and slip uncertainty exist in the Earth's crust. To what extent it
 19 influences crustal stress and its evolution is intriguing. We established a quasi-static, 2D model to
 20 simulate the stress evolution due to Coulomb frictional slips in the brittle crust. The model simply
 21 features randomly-oriented fractures with heterogeneous frictional coefficients. We emphasized
 22 the global stress response by summing the contribution of cascades of local frictional slip under
 23 specific boundary conditions. We illustrated that the decrease in stress difference manifests as a
 24 self-organized process that ultimately leads to frictional equilibrium. The model informs that the
 25 frictional equilibrium of a stochastic system can depart substantially from a deterministic
 26 estimation. Although the model quantitatively corroborates the notion of frictional equilibrium in
 27 places where fracture slip is the dominant mechanism for stress release, it reveals far more
 28 profound influence of system heterogeneity on the local and global stress evolution.

29

30 Plain Language Summary

31 Knowledge of crustal stress and its uncertainty is of fundamental importance to a wide range of
 32 problems. It is recognized that the intra-plate continental crust is generally in a state of frictional
 33 failure, the stress magnitudes of which usually cannot accumulate beyond the frictional strength.
 34 As a conventional practice, Coulomb theory is adopted together with laboratory-derived frictional
 35 coefficients for crustal stress estimations. Although it is able to attain a first-order agreement, such
 36 a practice has been primarily employed in a deterministic sense, which overlooks the fact that
 37 stress distribution is highly complex and spatially heterogeneous at different scales in the Earth's
 38 crust. In addition, how the upper crust keeps its stress magnitudes at its frictional strength is yet
 39 well understood. To this end, we proposed a simple quasi-static 2D model with distributed
 40 frictional coefficient as a proxy of the intrinsic system heterogeneity. By quantitatively
 41 investigating the global-scale stress evolution due to stochastic, local-scale frictional slips, this
 42 study shows that the magnitudes and uncertainties of both local- and global-scale stresses of the
 43 system can be greatly controlled by its friction heterogeneity. This model is believed to quantify
 44 and extend the classic notion of frictional equilibrium within the brittle crust.

45

46 1 Introduction

47 Fault slip is one of the dominant mechanisms for stress release in the Earth's upper crust.
 48 The stress of the fractured crust is often considered under 'frictional equilibrium', a dynamic status
 49 induced by ongoing tectonic/gravity loading and resulting fault slips (Zoback and Townend, 2001).
 50 Via the simple Coulomb frictional failure theory, the limiting state of stress can be conveniently
 51 expressed as:

$$52 \quad \sigma_1/\sigma_3 = \left(\sqrt{\mu^2+1}+\mu\right)^2 \quad (1)$$

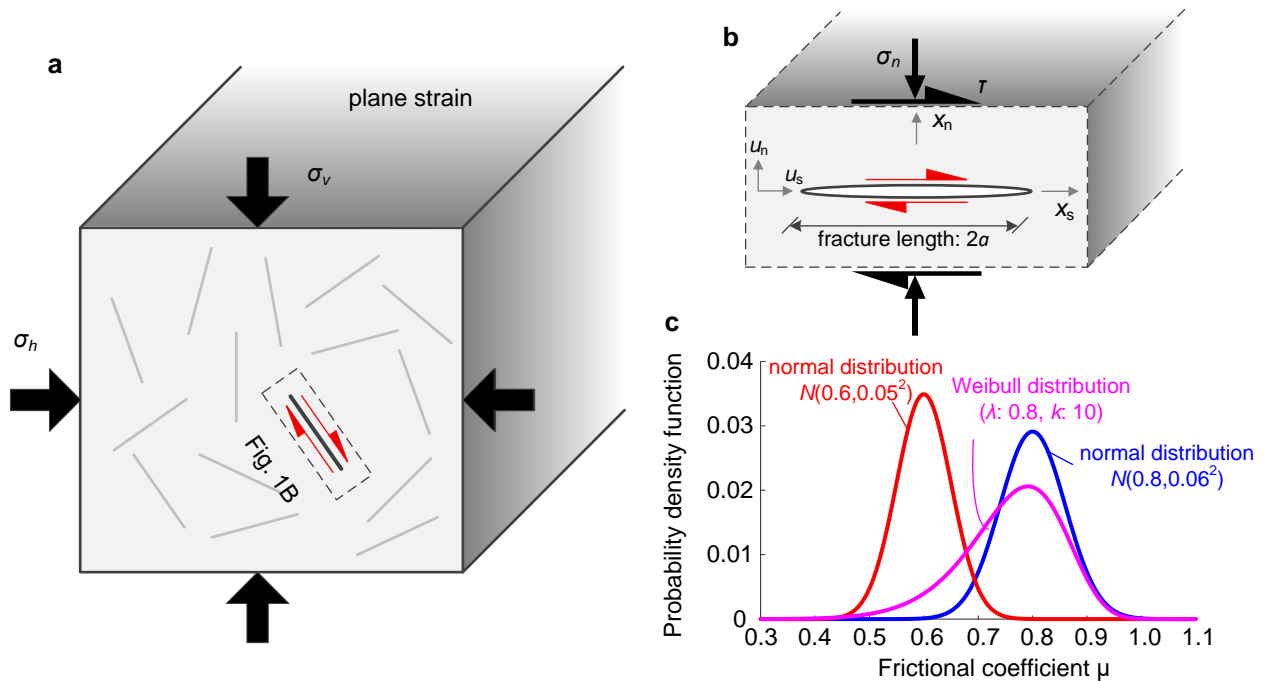
53 where σ_1 and σ_3 are the effective major and minor principal stress, respectively, and μ is the
 54 frictional coefficient. Adopting laboratory-derived frictional coefficient values ($\mu = 0.6-1.0$)
 55 (Byerlee, 1978), Eq.(1) has enabled the estimation of in situ stress and vice versa, the analysis of
 56 fault criticality (Brace and Kohlstedt, 1980; Townend and Zoback, 2000). However, to what spatial
 57 and temporal scale a deterministic use of Eq.(1) applies to is questionable, and has been often

58 misused and mis-interpreted. Evidently, the value of μ varies spatially and temporally in the
 59 Earth's crust (Dieterich, 1979; Rivera and Kanamori, 2002), which underscores that such
 60 variability in a natural system must be considered.

61 To reflect such variability, recent attempts in stress estimation and/or fault slip analysis
 62 incorporated uncertainties in geomechanical parameters with a probabilistic approach (e.g., Walsh
 63 and Zoback, 2016; Hosseini et al., 2018; Luo and Ampuero, 2018), which offers more insights
 64 than a pure deterministic application of Eq.(1). However, one aspect still missing from existing
 65 stress models is how such system variability and heterogeneity influence the evolution of the in
 66 situ stress. How fault slip leads to frictional equilibrium, if possible, and whether it is attained is
 67 intriguing. The understanding of this evolution requires not only the influence of the far-field stress
 68 on the local fault slip, but also the feedback from the local slip to the global stress release. In this
 69 paper, we present a quasi-static, 2D model to simulate the stress evolution due to Coulomb
 70 frictional slip in the crustal rock masses. We explicitly consider frictional coefficient
 71 heterogeneity, as a proxy of the combined system uncertainties and variabilities, and emphasize
 72 the connection between the global and local stress response.

73 2 Methods

74 2.1 Model Configuration



75 **Figure 1.** **a** Schematics of the plane strain model: randomly-distributed fractures in an elastic
 76 matrix subject to uniform stresses at the boundary. **b** Close-up of a fracture with its geometrical
 77 and mechanical features. **c** Distributions of frictional coefficient (μ) of fractures adopted to in the
 78 model.
 79
 80

81 The model we present is a fractured, elastic matrix configured under plane strain condition
 82 (Figure 1A). The embedded fractures are linear, planar, and cohesion-less. They are perpendicular
 83 to the plane section and through-going. The fractures are spatially characterized only by their

84 orientations and their actual positions in the plane are irrelevant, see Text S1. This treatment
 85 follows Wiebols and Cook (1968) and other work on effective medium (Kachanov, 1992; Davy et
 86 al., 2018). Deemed essential to our model, the embedded fractures differ in their frictional
 87 coefficient μ , which can follow any arbitrary distribution, e.g., Figure 1C, as a proxy for the
 88 inherent heterogeneity in the system. The elastic matrix is simply characterized by its shear
 89 modulus G and Poisson's ratio ν . As a quasi-static model for stress relaxation of much longer time
 90 scales, complex dynamic issues such as fracture initiation, propagation and termination are not
 91 addressed.

92 2.2 Local Slip – Shear Displacement

93 Given a remotely applied effective stress tensor σ at the model boundary, local shear and
 94 normal stresses (σ_n and τ) acting on individual fractures are mathematically expressed via the unit
 95 normal and shear vector, \mathbf{n} and \mathbf{s} , of each fracture. We are cognizant of stress perturbation near
 96 fractures, but considered it trivial in the context of upscaling (see Text S1). We simply adopt the
 97 classic Coulomb frictional failure criterion to determine whether slip occurs on a fracture. If
 98 $\tau > \mu \cdot \sigma_n$, the fracture is identified as critical and frictional slip occurs, otherwise the fracture stays
 99 perfectly bonded, behaving as part of the elastic matrix with no relative displacement occurring
 100 between opposite fracture sides. We assume that the shear stress on the fracture will drop to its
 101 frictional resistance after the slip, so that the shear stress difference $\Delta\tau = \tau - \mu \cdot \sigma_n$ drives the
 102 relative displacement across the fracture.

103 Based on elastic crack theory (Pollard and Segall, 1987), the normal and shear
 104 displacements (u_n and u_s) on opposite sides of a fracture associated with the slip can be analyzed
 105 conveniently in the local fracture coordinates (x_n, x_s) (Figure 1B). Specifically, they are:

$$106 \quad u_n = \Delta\tau \frac{1-2\nu}{2G} x_s \quad (2a)$$

$$107 \quad u_s^\pm = \pm \Delta\tau \frac{1-\nu}{G} \sqrt{a^2 - x_s^2} \quad (2b)$$

108 where $x_s \in [-a, a]$, a is the fracture half-length, and the superscript ' \pm ' of u_s refers to
 109 displacement along the upper and lower fracture side ($x_n = \pm 0$), respectively. The average relative
 110 shear displacement between opposite sides $\bar{\mathbf{d}}_s$ is from integrating the relative shear displacement
 111 ($u_s^+ - u_s^-$) across the fracture length:

$$112 \quad \bar{\mathbf{d}}_s = \left(\frac{1}{a} \int_0^a \Delta\tau \frac{2(1-\nu)}{G} \sqrt{a^2 - x_s^2} dx_s \right) \mathbf{s} = \left(\Delta\tau \frac{a\pi(1-\nu)}{2G} \right) \mathbf{s} \quad (3a)$$

113 To reflect shear-induced dilatancy commonly observed in the brittle rock mass (Scholz,
 114 1974; Fielding et al., 2009), we utilize dilatancy factor β to relate $\bar{\mathbf{d}}_s$ to the average relative normal
 115 displacement $\bar{\mathbf{d}}_n$:

$$116 \quad \bar{\mathbf{d}}_n = \beta |\bar{\mathbf{d}}_s| \mathbf{n} = \beta \left(\Delta\tau \frac{a\pi(1-\nu)}{2G} \right) \mathbf{n} \quad (3b)$$

117 2.3 Upscaling Local Slips

118 We invoke Gaussian theorem (Hill, 1963; Kachanov, 1992) to relate the contribution of
 119 local displacement incurred by individual frictional slip to the global strain at the model boundary
 120 $\Delta\boldsymbol{\varepsilon}$:

121
$$\Delta\boldsymbol{\varepsilon} = \frac{a}{A} (\bar{\mathbf{d}} \otimes \mathbf{n} + \mathbf{n} \otimes \bar{\mathbf{d}}) \quad (4)$$

122 where A is the cross-section area of the model and $\bar{\mathbf{d}} = \bar{\mathbf{d}}_s + \bar{\mathbf{d}}_n$.

123 The total global strain at the model boundary comprises the strain of the intact elastic
124 matrix $\boldsymbol{\varepsilon}^m$ and, if critical fractures exist, the summed strain $\Delta\boldsymbol{\varepsilon}$ induced by successive, individual
125 slips of a cascade of critical fractures:

126
$$\boldsymbol{\varepsilon}_i = \boldsymbol{\varepsilon}^m + \sum_i \frac{a_i}{A} (\bar{\mathbf{d}}_i \otimes \mathbf{n}_i + \mathbf{n}_i \otimes \bar{\mathbf{d}}_i) \quad (5)$$

127 where subscript i denotes the i th fracture in a cascade of slips. The intact elastic matrix strain $\boldsymbol{\varepsilon}^m$ is
128 simply regulated by Hooke's law under plane strain. Details on the slip cascades and upscaling are
129 expanded in Text S2.

130 2.4 Slip Iterations, Time Steps

131 If stress and/or strain is mandated constant at the model boundary, the contribution of local
132 fracture slips requires adjustment of stress/strain in the intact elastic matrix. This entails global
133 stress adjustment at the model boundary and further modifies the criticality of individual fractures
134 locally, necessitating a frequent re-evaluation of the fracture criticality. To this end, we impose an
135 iterative process to accommodate the interplay between local fracture criticality, global stress and
136 strain, and fractured matrix, tailored to the model experimentation below of specific boundary
137 conditions (Text S2). We predicate the termination of the iteration when the shear stress difference
138 $\Delta\tau$ of the most critical fracture is below 0.01 MPa. Constant slip rate depending on the global
139 effective properties and local stress is assumed for each critical fracture within a time step, at the
140 end of which the contribution of multiple slips is summed by the non-interaction approximation
141 (Bristow, 1960) (expanded in Text S2).

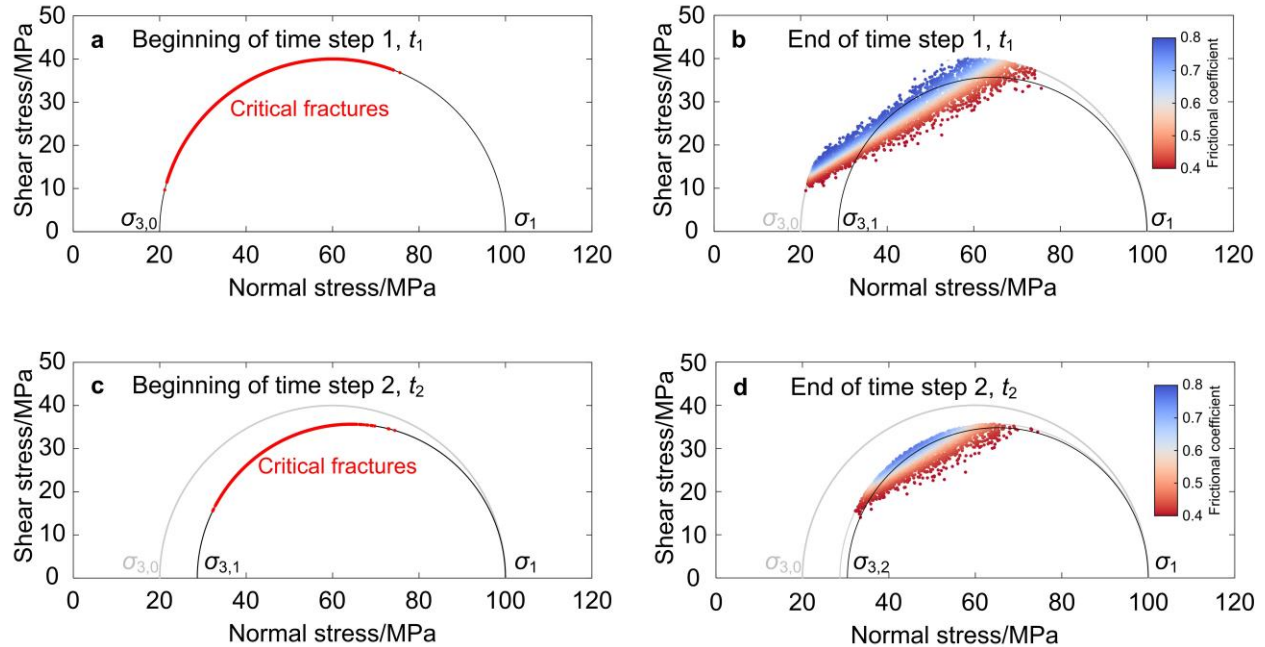
142 3 Results

143 3.1 Model Experimentation in the Context of Normal Faulting Stress Regime

144 We start experimenting our model by simulating the simple scenario of stable intra-plate
145 region with normal faulting stress environment ($\sigma_v = \sigma_1 > \sigma_h = \sigma_3$). The boundary condition is set
146 with constant vertical stress and constant lateral strain. We assign the model with size A of
147 100×100 (in unit length), and 10,000 randomly-oriented fractures with equal length ($a_i \equiv a = 1$,
148 unit length). The frictional coefficients of all fractures are normally distributed: the mean and the
149 standard deviation of the distribution are 0.6 and 0.05, respectively, i.e., $N(0.6, 0.05^2)$ shown in
150 Figure 1C. The dilatancy factor of fractures β is 0.05. The (intact) elastic matrix is assigned shear
151 modulus $G = 20$ GPa and Poisson's ratio $\nu = 0.3$.

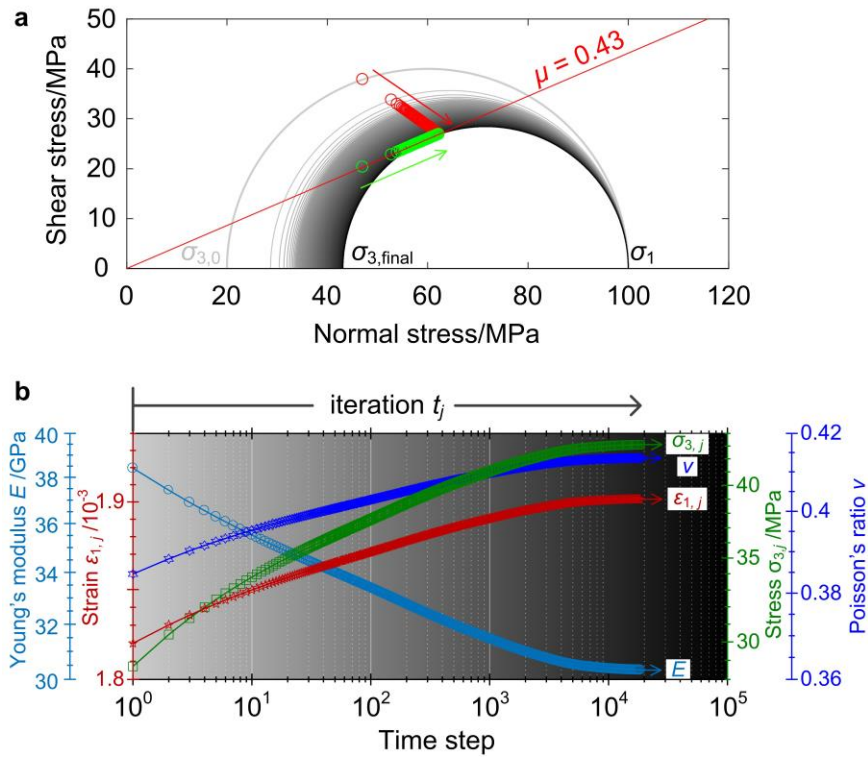
152 We arbitrarily apply an effective stress tensor $\boldsymbol{\sigma}$ ($\sigma_{3,0} = 20$ MPa, and $\sigma_{1,0} = 100$ MPa) at the
153 model boundary instantaneously at initial time t_0 . It will become clear later in the text that the
154 starting stress difference hardly matters to the final frictional equilibrium. Since no fracture slip
155 occurs at t_0 , $\varepsilon_{1,0}$ and $\varepsilon_{3,0}$ at the model boundary are only related to the elastic matrix response, i.e.,
156 $\varepsilon_{1,0} = \varepsilon_1^m$ and $\varepsilon_{3,0} = \varepsilon_3^m$. An initial evaluation of fracture criticality allows the iterative slip process
157 to begin. Mohr diagrams are used to illustrate the first two time steps as an example (Figure 2).
158 The slip of critical fractures reduces the shear stresses on themselves to their frictional resistance,
159 revealing local stress heterogeneities in the system. Upon the end of a time step, i.e., a cascade of
160 slips, boundary stress σ_3 is increased to maintain constant lateral strain and fracture criticality

161 evaluation re-iterates. With the starting stress difference substantially above the possible
 162 equilibrium state, the stress evolution undergoes multiple time steps (1, 2, ..., j , ...) before it
 163 terminates (see details in Text S2). As the vertical stress σ_1 is held constant, the horizontal stress
 164 $\sigma_{3,j}$ increases, or, the stress difference ($\sigma_{1,j} - \sigma_{3,j}$) relaxes monotonically. The stress evolution at
 165 the model boundary manifests itself as a series of contracting Mohr diagrams (Figure 3A). The
 166 number of fracture slips and the amount of stress relaxation of each time step diminishes
 167 significantly as the iteration continues. Numerous fracture slips induce the accumulation of vertical
 168 strain and the reduction of system stiffness, as illustrated in Figure 3B. Such response is
 169 characteristic of the absence of tectonic loading.



170
 171 **Figure 2.** Mohr diagrams illustrating the first two iterations of stress evolution from an arbitrary,
 172 initial stress condition within the normal faulting stress regime. The fractures in the system follow
 173 a normally distributed frictional coefficient $N(0.6, 0.05^2)$. **a, c:** Beginning each time step, critical
 174 fractures (red) are identified. **b, d:** After a cascade of local fracture slips within the time step, shear
 175 stress of each critical fracture drops to its frictional resistance, which results in the global stress
 176 update, i.e., σ_3 increase.

177 The model's final stress state, or frictional equilibrium, is attained when iterations
 178 terminate. The most critical fracture in the system can be located. Retrospectively, the stress state
 179 and frictional resistance of the most critical fracture through the iterations can be traced, as
 180 illustrated in Figure 3A. Evidently, the fracture keeps slipping as long as its shear stress is larger
 181 than but converges towards its frictional resistance. The linear trace of the fracture frictional
 182 resistance can be interpreted as the equivalent frictional strength of the system, that is, $\mu = 0.43$.



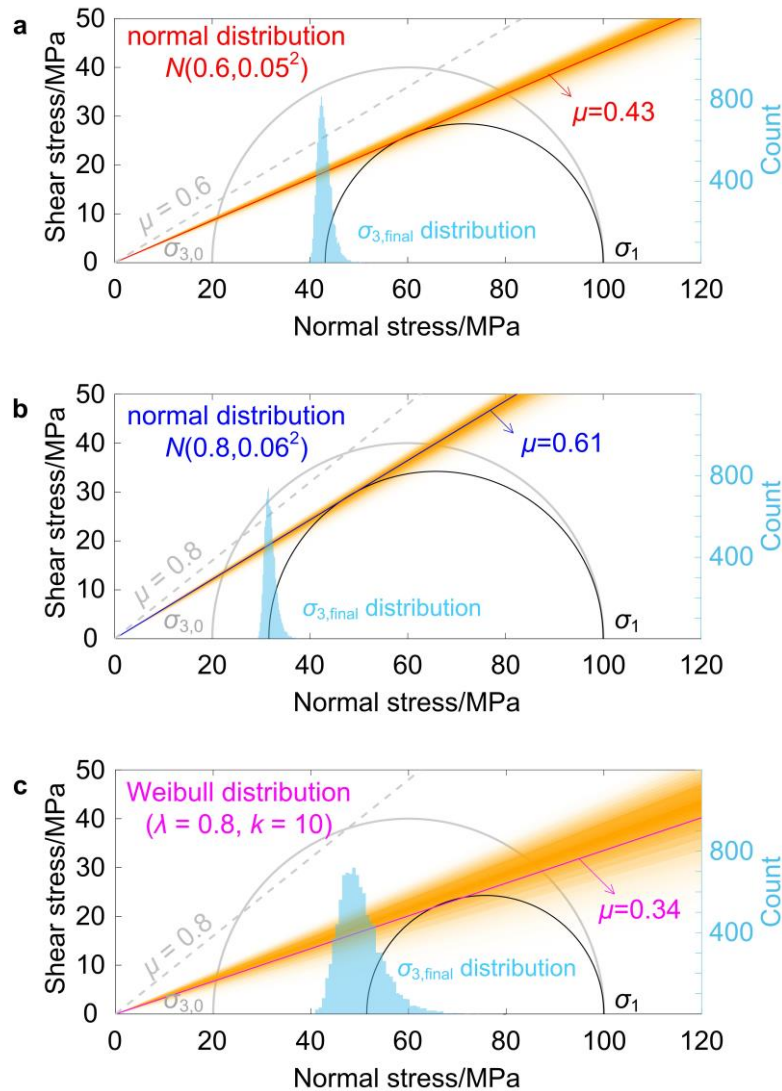
183 **Figure 3.** Overview of the temporal evolution of the model specified in Figure 2. **a** The stress
 184 relaxation due to cascades of fracture slips is illustrated by contracting Mohr diagrams. The final
 185 stress state rests on the frictional envelop ($\mu = 0.43$), which is in fact controlled by the most critical
 186 fracture in the system. Red and green circles represent the resolved stress state and frictional
 187 resistance on the most critical fracture at each time step. **b** Evolving stress (σ), strain (ϵ), Young's
 188 modulus (E), and Poisson's ratio (ν) through iterations. Note the rate of change in these parameters
 189 gradually diminishes towards the final stress state. Gray scale color scheme in **a** and **b** corresponds
 190 to iterations (logarithmic).
 191

192 3.2 More on Heterogeneous Frictional Coefficient

193 Comparing this stochastic treatment with the deterministic case in which the frictional
 194 coefficients of all fractures are homogeneous ($\mu = 0.6$, see Text S3), the final σ_3 upon equilibrium
 195 of the former is smaller than that of the latter, intuitively indicated in Figure 4A. Apparently, the
 196 maximum stress difference that can be sustained by the stochastic system does not depend on the
 197 mean or the upper bound of the frictional coefficient distribution. This is further demonstrated by
 198 two additional distributions, i.e., normal distribution $N(0.8, 0.06^2)$ and Weibull distribution with
 199 scale parameter $\lambda = 0.8$ and shape parameter $k = 10$, as illustrated in Figure 4B and 4C,
 200 respectively.

201 Further reviewing the stress evolution of each distribution, we identified that the frictional
 202 coefficient of the most critical fracture does not necessarily correspond to the lowest value, as one
 203 would assume, but it is located close to the lower bound of the distribution. Monte Carlo
 204 simulations shows such an observation is of high probability (Text S4). This suggests that the most
 205 critical fracture is determined jointly by its frictional coefficient and orientation with respect to the
 206 global stress. That said, the equivalent frictional strength of the fractured matrix is dependent on
 207 the combination of frictional coefficient distribution and orientations of all fractures. As indicated

208 by Figure 4, the uncertainty of the equivalent frictional strength becomes more evident when the
 209 μ distribution departs further from uniformity, which also implies the degree of heterogeneity of
 210 global stress in such a stochastic system. Therefore, when inferring the state of stress in situ
 211 assuming frictional equilibrium, the practical value of frictional coefficient to be adopted is of utter
 212 importance.



213 **Figure 4.** Initial (gray) and final (black) stress state for the same model configuration but different
 214 frictional coefficient distributions. The most probable final stress state, bounded by the
 215 corresponding equivalent frictional coefficient of the system, is associated with uncertainties
 216 (fuzzy lines or the distribution of σ_3 , see Figure S6 for more details).
 217

218 4 Conclusions

219 The model extends the notion of frictional equilibrium. For the deterministic interpretation
 220 in which the frictional coefficient is homogeneous, the frictional equilibrium refers to a state
 221 prescribed by Eq. (1). In a heterogeneous system, the frictional equilibrium can be understood as
 222 a dynamic process as illustrated in the model experimentation, spanning from the very first
 223 frictional slip to the final one possibly allowed by the prevailing in situ stress difference. The use

224 of Eq. (1) in this instance therefore incurs great uncertainty. Informed by the numerous time steps
 225 leading to the final frictional equilibrium, the most critical fracture or fault stays critical while the
 226 rest of the crust experiences practically few slips, i.e., little global stress reduction. The apparent
 227 discrepancy between the local and global response reflects the stress heterogeneity within the
 228 system, which is jointly regulated by the variability of frictional coefficient and orientation of the
 229 fractures. To this end, the controversy over whether the upper crust is critically stressed is plausibly
 230 resolved. Again, we emphasize that the dominant mechanism of stress release in this context is
 231 frictional slip. Other mechanisms that may further lower the stress difference below frictional
 232 equilibrium in certain lithologies, such as viscoplastic deformation in shales (Sone and Zoback,
 233 2014; Ma and Zoback, 2017), pressure solution in carbonates (Gunzburger and Cornet 2007;
 234 Gratier et al., 2013; Brantut et al., 2014), are not addressed here.

235 The evolution of stress reduction raises questions about the stage at which the current state
 236 of stress is with respect to the equilibrium. This is informative to stress estimation and fault slip
 237 tendency analysis. Note that in our model, the evolution iterates through ‘pseudo’ time steps and
 238 is not calibrated against real time. This is a compromise for computational feasibility and
 239 efficiency, so the interpretation in a temporal sense should be executed with caution. Nonetheless,
 240 the time-dependent stress reduction and matrix response appears to be reasonable and is deemed
 241 of first-order importance. Because of the difficulty to impose real time in the model, we were
 242 unable to experiment boundary conditions with prescribed strain or stress rate, which is more
 243 realistic in tectonically active regions. It is worth noting that no fracture interaction, extension and
 244 matrix damage was allowed in the model. If that was the case, the expected stress reduction will
 245 be more significant due to increased number and length of fractures and lowered equivalent matrix
 246 stiffness. The equivalent frictional strength of the crust will be even lower, in other words, the
 247 difference between the reality and the deterministic model will be more substantial.

248 **Acknowledgments**

249 This work is supported by Swiss National Science Foundation (grant No. 182150) and benefited
 250 from discussions with Norman Sleep and Hiroki Sone. This is a theoretical study and contains no
 251 collected data. The scripts used to produce the results can be requested from the authors.

252 **References**

- 253 Brace, W. F., & Kohlstedt, D. L. (1980). Limits on lithospheric stress imposed by laboratory
 254 experiments. *Journal of Geophysical Research: Solid Earth*, 85(B11), 6248-6252. doi:
 255 10.1029/JB085iB11p06248.
- 256 Brantut, N., Heap, M. J., Baud, P., & Meredith, P. G. (2014). Mechanisms of time-dependent
 257 deformation in porous limestone. *Journal of Geophysical Research: Solid Earth*, 119(7),
 258 5444-5463. doi: 10.1002/2014JB011186.
- 259 Bristow, J. R. (1960). Microcracks, and the static and dynamic elastic constants of annealed and
 260 heavily cold-worked metals. *British Journal of Applied Physics*, 11(2), 81.
- 261 Byerlee, J. (1978). Friction of rocks. In *Rock friction and earthquake prediction* (pp. 615-626).
 262 Birkhäuser, Basel. doi: 10.1007/978-3-0348-7182-2_4.
- 263 Davy, P., Darcel, C., Le Goc, R., & Mas Ivars, D. (2018). Elastic properties of fractured rock
 264 masses with frictional properties and power law fracture size distributions. *Journal of*
 265 *Geophysical Research: Solid Earth*, 123(8), 6521-6539. doi: 10.1029/2017JB015329.

- 266 Dieterich, J. H. (1979). Modeling of rock friction: 1. Experimental results and constitutive
267 equations. *Journal of Geophysical Research: Solid Earth*, 84(B5), 2161-2168. doi:
268 10.1029/JB084iB05p02161.
- 269 Fielding, E. J., Lundgren, P. R., Bürgmann, R., & Funning, G. J. (2009). Shallow fault-zone
270 dilatancy recovery after the 2003 Bam earthquake in Iran. *Nature*, 458(7234), 64-68. doi:
271 10.1038/nature07817.
- 272 Gratier, J. P., Dysthe, D. K., & Renard, F. (2013). The role of pressure solution creep in the
273 ductility of the Earth's upper crust. In *Advances in Geophysics* (Vol. 54, pp. 47-179). Elsevier.
274 doi: 10.1016/B978-0-12-380940-7.00002-0.
- 275 Grechka, V., & Kachanov, M. (2006). Effective elasticity of fractured rocks: A snapshot of the
276 work in progress. *Geophysics*, 71(6), W45-W58. doi: 10.1190/1.2360212.
- 277 Gunzburger, Y., & Cornet, F. H. (2007). Rheological characterization of a sedimentary formation
278 from a stress profile inversion. *Geophysical Journal International*, 168(1), 402-418. doi:
279 10.1111/j.1365-246X.2006.03140.x.
- 280 Healy, D. (2008). Damage patterns, stress rotations and pore fluid pressures in strike-slip fault
281 zones. *Journal of Geophysical Research: Solid Earth*, 113(B12). doi:
282 10.1029/2008JB005655.
- 283 Hill, R. (1963). Elastic properties of reinforced solids: some theoretical principles. *Journal of the
284 Mechanics and Physics of Solids*, 11(5), 357-372. doi: 10.1016/0022-5096(63)90036-X.
- 285 Hosseini, S. M., Goebel, T. H. W., Jha, B., & Aminzadeh, F. (2018). A Probabilistic Approach to
286 Injection-Induced Seismicity Assessment in the Presence and Absence of Flow Boundaries.
287 *Geophysical Research Letters*, 45(16), 8182-8189. doi: 10.1029/2018GL077552.
- 288 Kachanov, M. (1992). Effective elastic properties of cracked solids: critical review of some basic
289 concepts. *Applied Mechanics Reviews*, 45(8), 304-335. doi: 10.1115/1.3119761.
- 290 Katz, O., & Reches, Z. E. (2004). Microfracturing, damage, and failure of brittle granites. *Journal
291 of Geophysical Research: Solid Earth*, 109(B1). doi: 10.1029/2002JB001961.
- 292 Luo, Y., & Ampuero, J. P. (2018). Stability of faults with heterogeneous friction properties and
293 effective normal stress. *Tectonophysics*, 733, 257-272. doi: 10.1016/j.tecto.2017.11.006.
- 294 Ma, X., & Zoback, M. D. (2017). Lithology-controlled stress variations and pad-scale faults: A
295 case study of hydraulic fracturing in the Woodford Shale, OklahomaWoodford Shale case
296 study. *Geophysics*, 82(6), ID35-ID44. doi: 10.1190/geo2017-0044.1.
- 297 Napier, J. A. L., & Malan, D. F. (1997). A viscoplastic discontinuum model of time-dependent
298 fracture and seismicity effects in brittle rock. *International Journal of Rock Mechanics and
299 Mining Sciences*, 34(7), 1075-1089. doi: 10.1016/S1365-1609(97)90201-X.
- 300 Perzyna, P. (1966). Fundamental problems in viscoplasticity. In *Advances in applied mechanics*
301 (Vol. 9, pp. 243-377). Elsevier.
- 302 Pollard, D. D., & Segall, P. (1987). Theoretical displacements and stresses near fractures in rock:
303 with applications to faults, joints, veins, dikes, and solution surfaces. In *Fracture mechanics
304 of rock* (pp. 277-347).

- 305 Rivera, L., & Kanamori, H. (2002). Spatial heterogeneity of tectonic stress and friction in the crust.
306 *Geophysical research letters*, 29(6), 12-1. doi: 10.1029/2001GL013803.
- 307 Ruina, A. L. (1980). Friction laws and instabilities: a quasi-static analysis of some dry friction
308 behaviour. *Ph. D. thesis, Division of Engineering, Brown University*.
- 309 Scholz, C. H. (1974). Post-earthquake dilatancy recovery. *Geology*, 2(11), 551-554. doi:
310 10.1130/0091-7613(1974)2<551:PDR>2.0.CO;2.
- 311 Sleep, N. H. (2006). Real contacts and evolution laws for rate and state friction. *Geochemistry,*
312 *Geophysics, Geosystems*, 7(8). doi: 10.1029/2005GC001187.
- 313 Sone, H., & Zoback, M. D. (2014). Time-dependent deformation of shale gas reservoir rocks and
314 its long-term effect on the in situ state of stress. *International Journal of Rock Mechanics and*
315 *Mining Sciences*, 69, 120-132. doi: 10.1016/j.ijrmms.2014.04.002.
- 316 Townend, J., & Zoback, M. D. (2000). How faulting keeps the crust strong. *Geology*, 28(5), 399-
317 402. doi: 10.1130/0091-7613(2000)28<399:HFKTCS>2.0.CO;2.
- 318 Walsh III, F. R., & Zoback, M. D. (2016). Probabilistic assessment of potential fault slip related
319 to injection-induced earthquakes: Application to north-central Oklahoma, USA. *Geology*,
320 44(12), 991-994. doi: 10.1130/G38275.1.
- 321 Wiebols, G. A., & Cook, N. G. W. (1968, November). An energy criterion for the strength of rock
322 in polyaxial compression. In *International Journal of Rock Mechanics and Mining Sciences*
323 *& Geomechanics Abstracts* (Vol. 5, No. 6, pp. 529-549). Pergamon. doi: 10.1016/0148-
324 9062(68)90040-5.
- 325 Zoback, M. D., & Townend, J. (2001). Implications of hydrostatic pore pressures and high crustal
326 strength for the deformation of intraplate lithosphere. *Tectonophysics*, 336(1-4), 19-30. doi:
327 10.1016/S0040-1951(01)00091-9.
328